Monthly Notices of the ROYAL ASTRONOMICAL SOCIETY

MNRAS **505,** 5714–5724 (2021) https://doi.org/10.1093/mnras/stab1642
Advance Access publication 2021 June 10

Galaxy clustering in harmonic space from the dark energy survey year 1 data: compatibility with real-space results

F. Andrade-Oliveira [1,2]★ H. Camacho [1,2] L. Faga,[2,3] R. Gomes,[2,3] R. Rosenfeld,[2,4] A. Troja,[2,4] O. Alves,[1,2,5] C. Doux [6] J. Elvin-Poole,[7,8] X. Fang [9] O. Friedrich,[10,11] N. Kokron,[12,13] M. Lima,[2,3] V. Miranda,[9] S. Pandey,[6] A. Porredon,[7,14,15] J. Sanchez,[16] M. Aguena [2,3] S. Allam,[16] J. Annis,[16] S. Avila [17] E. Bertin [18,19] D. Brooks,[20] D. L. Burke,[13,21] M. Carrasco Kind [22,23] J. Carretero [24] R. Cawthon,[25] C. Chang [26,27] A. Choi,[7] M. Costanzi,[28,29,30] M. Crocce [14,15] L. N. da Costa,[2,31] M. E. S. Pereira,[5] S. Desai,[32] H. T. Diehl,[16] P. Doel,[20] A. Drlica-Wagner,[16,26,27] S. Everett,[33] A. E. Evrard [5,34] I. Ferrero [35] J. Frieman,[16,27] J. García-Bellido [17] E. Gaztanaga [14,15] D. W. Gerdes,[5,34] D. Gruen [12,13,21] R. A. Gruendl,[22,23] S. R. Hinton [36] D. L. Hollowood [33] B. Jain,[6] D. J. James,[37] N. Kuropatkin,[16] O. Lahav,[20] N. MacCrann [38] M. A. G. Maia,[2,31] M. March [6] P. Melchior [39] F. Menanteau,[22,23] R. Miquel,[24,40] R. Morgan,[25] J. Myles [12,13,21] R. L. C. Ogando [2,31] A. Palmese [16,27] F. Paz-Chinchón,[22,41] A. A. Plazas Malagón [39] M. Rodriguez-Monroy,[42] E. Sanchez,[42] V. Scarpine,[16] S. Serrano,[14,15] I. Sevilla-Noarbe,[42] M. Smith [43] M. Soares-Santos,[5] E. Suchyta [44] G. Tarle,[5] C. To[12,13,21] and (DES Collaboration)

Affiliations are listed at the end of the paper

Accepted 2021 June 4. Received 2021 May 27; in original form 2021 April 8

ABSTRACT

We perform an analysis in harmonic space of the Dark Energy Survey Year 1 Data (DES-Y1) galaxy clustering photometric data using products obtained for the real-space analysis. We test our pipeline with a suite of lognormal simulations, which are used to validate scale cuts in harmonic space as well as to provide a covariance matrix that takes into account the DES-Y1 mask. We then apply this pipeline to DES-Y1 data taking into account survey property maps derived for the real-space analysis. We compare with real-space DES-Y1 results obtained from a similar pipeline. We show that the harmonic space analysis we develop yields results that are compatible with the real-space analysis for the bias parameters. This verification paves the way to performing a harmonic space analysis for the upcoming DES-Y3 data.

Key words: cosmology: observations – large-scale structure of Universe.

1 INTRODUCTION

Cosmology has matured into a precision, data-driven science in the last couple of decades. An immense amount of data from different observables, including the detailed study of the cosmic microwave background, the abundance of light elements, the detection of thousands of Type Ia supernovae and the distribution of galaxies and their shapes as measured in large galaxy surveys has confirmed the standard spatially flat ΛCDM cosmological model (e.g. Frieman, Turner & Huterer 2008). There are, however, some tensions among some of these observables that, if they stand, can point to important modifications in our understanding of the universe (Verde, Treu & Riess 2019). Therefore, the testing of the standard cosmological model and the search for new phenomena continue with new data and improved analysis methods.

The main cosmological analysis of several recent galaxy surveys uses the measurement of two-point correlation functions (or power spectra) of observables, such as galaxy clustering and cosmic shear, as inputs to the estimation of cosmological parameters of a given model in a likelihood framework. The use of a joint combination of these two-point correlations is conventionally called the '3 × 2-point' analysis including galaxy–galaxy, galaxy–galaxy lensing, and galaxy lensing–galaxy lensing (shear) two-point correlations. These analyses can be performed in real-space with the angular correlation functions or in harmonic space with the angular power spectra. There are advantages and disadvantages in both approaches. For an idealized full-sky survey, the harmonic modes are independent on linear scales and the covariance matrices are diagonal. This is not the case in real space, where the angular correlation function presents large correlations at different angular scales. For realistic surveys, however, the effect of the survey mask introduces mode coupling that makes the analyses more convoluted and the real-space measurements are in general more amenable to the presence of the

★ E-mail: felipe.andrade-oliveira@unesp.br

mask. In principle the data contains the same amount of information whether it is analysed in real or harmonic space if all modes or scales are included but in reality differences may arise due to finite survey area and the different, independent methods that are used (e.g. the definition of scale cuts).

The Dark Energy Survey (DES[1]) used photometric redshift measurements to perform tomographic real-space analyses of galaxy clustering (Elvin-Poole et al. 2018), cosmic shear (Troxel et al. 2018), and galaxy–galaxy lensing (Prat et al. 2018), culminating in a joint 3×2-point analysis (Abbott et al. 2018) for its first year of data (DES-Y1). The only harmonic space analysis from DES-Y1 data so far was the study of baryon acoustic oscillations (Abbott et al. 2019b; Camacho et al. 2019).

Other photometric surveys have recently presented results in harmonic space. The Kilo-Degree Survey (KiDS[2]) has presented a harmonic- and real- space analysis of cosmic shear (Köhlinger et al. 2017) and 3×2-point analysis also in harmonic space in combination with different data sets (van Uitert et al. 2018; Heymans et al. 2020). Balaguera-Antolínez et al. (2018) investigated the clustering in harmonic space in the local Universe using the 2MASS Photometric Redshift catalogue (2MPZ; Bilicki et al. 2014). The Subaru Hyper Suprime-Cam (HSC[3]) has performed a cosmic shear analysis from its first year of data both in harmonic (Hikage et al. 2019) and real-space (Hamana et al. 2020). Recently, Nicola et al. (2020) undertook an independent investigation of the galaxy clustering in harmonic space using HSC public data.

We should also mention that in spectroscopic surveys the clustering analyses are performed in three dimensions, since they have access to more reliable spectroscopic redshift measurements. The most recent results come from the completed Sloan Digital Sky Survey IV (SDSS-IV) extended Baryon Oscillation Spectroscopic Survey, eBOSS[4] (eBOSS Collaboration 2020) using both the two-point correlation function (Tamone et al. 2020; Bautista et al. 2021; Hou et al. 2021) and the power spectrum (de Mattia et al. 2020; Gil-Marín et al. 2020; Neveux et al. 2020) for different tracers (luminous red galaxies, emission line galaxies, and quasars). In addition, two-dimensional angular clustering analysis with SDSS data were also performed with the DR12 data, using both the angular correlation function (Salazar-Albornoz et al. 2017) and the angular power spectrum (Loureiro et al. 2019).

We perform an analysis in harmonic space of galaxy clustering from DES-Y1 data using the galaxy sample and the survey systematic maps with the corresponding weights from the real-space analysis (Elvin-Poole et al. 2018). In order to compare the harmonic space analysis with the real space one we adopt the same fiducial cosmology used in Elvin-Poole et al. (2018), namely a flat ΛCDM model with cosmological parameters $\Omega_m = 0.276$, $h_0 = 0.7506$, $\Omega_b = 0.0531$, $n_s = 0.9939$, $A_s = 2.818378 \times 10^{-9}$, and $\Omega_\nu h^2 = 0.00553$. This will be referred to as DES-Y1 cosmology. In this cosmology the amplitude of perturbations is fixed at $\sigma_8 = 0.83$. Our main goal is to develop and test the tools for the harmonic space analyses of galaxy clustering, demonstrating the compatibility with the DES-Y1 results in real space.

This paper is organized as follows. In Section 2, we describe the theoretical modelling of the angular power spectrum, presenting in Section 3 the pseudo-C_ℓ method used to measure the angular power spectrum in a masked sky. Section 4.1 details the generation of lognormal mocks. The results of measurements of the galaxy clustering in the mocks are shown in Section 4.2 and different covariance matrices are compared in Section 5. The pipeline that we develop for the estimation of parameters from the angular power spectrum is presented in Section 6 where we discuss the adopted scale cuts and it is applied on the mocks in 7. Finally, Section 8 shows our results on DES-Y1 data and we present our conclusions in Section 9.

2 THEORETICAL MODELLING

The starting point of the modelling of the galaxy angular power spectrum is the 3D nonlinear matter power spectrum $P(k, z)$ at a given wavenumber k and redshift z. The matter power spectrum may be obtained from public available Boltzmann solvers, e.g. CAMB[5] or CLASS,[6] in order to calculate the linear power spectrum and the late-time nonlinear power spectrum with the HALOFIT fitting formula (Smith et al. 2003) in its updated version (Takahashi et al. 2012). The galaxy angular power spectrum function can then be derived from this 3D power spectrum in the Limber approximation (Limber 1953; LoVerde & Afshordi 2008) as (e.g. Krause et al. 2017):

$$C^{ij}_{\delta_g\delta_g}(\ell) = \int \mathrm{d}\chi \, \frac{q^i_g\left(\frac{\ell+\frac{1}{2}}{\chi}, \chi\right) q^j_g\left(\frac{\ell+\frac{1}{2}}{\chi}, \chi\right)}{\chi^2} P\left(\frac{\ell+\frac{1}{2}}{\chi}, z(\chi)\right), \tag{1}$$

where χ is the comoving radial distance, i and j denote different combinations of photometric redshift bins and the radial weight function for clustering q^i_g is given by

$$q^i_g(k, \chi) = b^i(k, z(\chi))\, n^i_g(z(\chi)) \frac{\mathrm{d}z}{\mathrm{d}\chi} . \tag{2}$$

Here H_0 is the Hubble parameter today, Ω_m the ratio of today's matter density to today's critical density of the universe, $z(\chi)$ is the redshift at comoving distance χ and $b^i(k, z)$ is a scale and redshift-dependent galaxy bias. Furthermore, $n^i_g(z)$ denote the redshift distributions of the DES-Y1 lens galaxies, normalized such that

$$\int \mathrm{d}z \; n^i_g(z) = 1 . \tag{3}$$

Here we assume a simple linear bias model, constant for each redshift bin, i.e. $b^i(k, z) = b^i$, as was adopted in all the fiducial analyses of the first year of DES data. To be consistent with the configuration-space analysis, our model assumes the Limber approximation and neglects redshift-space distortions terms following Elvin-Poole et al. (2018). The validity of these assumptions for the DES-Y1 analysis choices were addressed in Krause et al. (2017) as a stress-test for the baseline model. The test was performed by generating a theory data vector without relying on the Limber approximation and properly including redshift-space distortion terms that was then analysed using the baseline choices for the DES-Y1 pipeline. Fig. 8 in Krause et al. (2017) demonstrates that the effect of the assumption of this approximation is negligible for recovering Ω_m and S_8 parameters for ΛCDM and w for wCDM.

The largest scale considered in the configuration space analysis was $\theta_{\rm max} = 250'$. In order to make our analysis consistent with this

[1] www.darkenergysurvey.org
[2] kids.strw.leidenuniv.nl
[3] hsc.mtk.nao.ac.jp/ssp
[4] www.sdss.org/surveys/eboss/

[5] camb.info
[6] www.class-code.net

result, we translate this scale to an $\ell_{\rm min} \sim \pi/\theta_{\rm max} = 43$. We study the small-scale cuts in harmonic space in Section 6.2.

When comparing with data, the angular power spectrum $C(\ell)$ should be binned in a given set of multipole ranges $\Delta\ell$. This binning and the effect of the mask will be discussed in Section 3.

The galaxy angular correlation function $w(\theta)$ can be computed from the angular power spectrum in the flat-sky approximation as

$$w(\theta)^{ij} = \int \frac{{\rm d}\ell\ell}{2\pi} J_0(\ell\theta) C^{ij}_{\delta_g\delta_g}(\ell), \tag{4}$$

where J_0 is the zeroth-order Bessel function of the first kind.

3 ESTIMATORS FOR TWO-POINT GALAXY CLUSTERING CORRELATIONS

In this section, we present the estimators used for the measurements of the two-point galaxy power spectrum and angular correlation functions. Our starting point is the fluctuation in the number density of galaxies in the direction $\hat{n}$ with respect to the average number density in the observed sample defined as

$$\delta_g(\hat{n}) = \frac{n_g(\hat{n}) - \bar{n}_g}{\bar{n}_g}. \tag{5}$$

In full sky, the fluctuation in the number density in a given position on the sphere $\delta_g(\hat{n})$ can be expanded in spherical harmonics $Y_{\ell m}(\hat{n})$ as

$$\delta_g(\hat{n}) = \sum_{\ell,m} a_{\ell m} Y_{\ell m}(\hat{n}). \tag{6}$$

The angular power spectrum C_ℓ is defined as

$$\left\langle a_{\ell' m'} a^*_{\ell m} \right\rangle = \delta_{\ell',\ell}\delta_{m',m} C_\ell. \tag{7}$$

The angular power spectrum can be estimated as

$$\hat{C}_\ell = \frac{1}{2\ell+1} \sum_m |a_{\ell m}|^2. \tag{8}$$

However, when the survey does not cover the full sky, the procedure above can still be carried out but it would result in the so-called pseudo-C_ℓ, denoted by $\tilde{C}_\ell$. In partial sky, the spherical harmonics are not orthogonal anymore and a mixture of ℓ modes contributes to the true power spectrum. The survey area is characterized by a mask that gives weights to the different regions of the survey. We use the pseudo-C_ℓ method developed in Hivon et al. (2002) and implemented in code `NaMaster` [7] (Alonso et al. 2019) to recover the true C_ℓ's by means of the so-called coupling matrix M

$$\tilde{C}_\ell = \sum_{\ell'} M_{\ell'\ell} C_{\ell'}. \tag{9}$$

The coupling matrix is solely determined by the survey mask and can be computed numerically in terms of Wigner 3j symbols by `NaMaster`. One needs to invert the coupling matrix or alternatively to forward-model the pseudo-C_ℓ to use in a likelihood analyses. We will use the former approach. In general, the loss of information due to the masked data makes it impossible to invert the coupling matrix (Alonso et al. 2019). A usual strategy to circumvent this difficulty is to bin the pseudo-C_ℓ into bandpowers.

We will model the angular power spectrum with a given binning of ℓ's and denote the binned angular power spectrum by C_q, where q defines a range of ℓ's, $\{\ell^1_q, \ell^2_q, \ldots, \ell^{n_q}_q\}$, and n_q is the number of modes grouped in that particular bin. The binned pseudo-C_ℓ in a bin q can be written as

$$\tilde{C}_q = \sum_{\ell\in q} w^\ell_q \tilde{C}_\ell, \tag{10}$$

where w^ℓ_q is a weight for each ℓ-mode normalized as $\sum_{\ell\in q} w^\ell_q = 1$. Unless otherwise stated we will adopt equal weights. The binned angular power spectrum is given by

$$\tilde{C}_q = \sum_{q'} \mathcal{M}_{qq'} C_{q'}, \tag{11}$$

where the binned coupling matrix is written as

$$\mathcal{M}_{qq'} = \sum_{\ell\in q} \sum_{\ell'\in q'} w^\ell_q M_{\ell'\ell}. \tag{12}$$

Inverting the binned coupling matrix is numerically more stable compared to the unbinned matrix.

The theoretical prediction for the binned power spectrum should be corrected as (Alonso et al. 2019)

$$C^{th}_q = \sum_l \mathcal{F}_{q\ell} C^{th}_\ell, \tag{13}$$

where the filter matrix $\mathcal{F}$ is given by

$$\mathcal{F}_{q\ell} = \sum_{qq'} \mathcal{M}^{-1}_{qq'} \sum_{\ell'\in q'} w^{\ell'}_{q'} M_{\ell'\ell}. \tag{14}$$

We also estimate the two-point angular correlation function $w(\theta)$ between the galaxy distribution in 2 directions separated by an angle θ

$$w(\theta) = \langle \delta_g(\hat{n}+\hat{\theta})\delta_g(\hat{n})\rangle, \tag{15}$$

where θ is the angle between directions $\hat{n}$ and $\hat{n}+\hat{\theta}$.

The effect of the partial sky is taken into account by computing correlations of galaxies in the actual catalogue and also from a random catalogue within the survey area.

We use the Landy–Szalay estimator (Landy & Szalay 1993) to estimate the galaxy clustering correlation function in a given angular bin $[\theta_1, \theta_2]$ as

$$\hat{w}[\theta_1,\theta_2] = \frac{DD[\theta_1,\theta_2] - 2DR[\theta_1,\theta_2] + RR[\theta_1,\theta_2]}{RR[\theta_1,\theta_2]}, \tag{16}$$

where, for the angular bin, $DD[\theta_1, \theta_2]$ is the number of pairs of galaxy, $RR[\theta_1, \theta_2]$ is the (normalized) number of pairs of random points sampling uniformly the survey footprint, and $DR[\theta_1, \theta_2]$ is the (normalized) number of galaxy-random-point pairs. In order to reduce the shape noise, the number density of random points n_r is set to be much larger than the number density of observed galaxies n_g. In this case, RR and DR are respectively rescaled by the factors $(n_g/n_r)^2$ and (n_g/n_r).

4 DES-Y1 MOCKS

4.1 Description of the mocks

We use a suite of 1200 lognormal simulations generated using the Full-sky Lognormal Astro-fields Simulation Kit (FLASK[8]) (Xavier, Abdalla & Joachimi 2016) for the DES-Y1 analyses with resolution Nside=4096. The input matter angular power spectra were computed using CosmoLike (Krause & Eifler 2017) with a flat ΛCDM model

[7] github.com/LSSTDESC/NaMaster

[8] www.astro.iag.usp.br/~flask

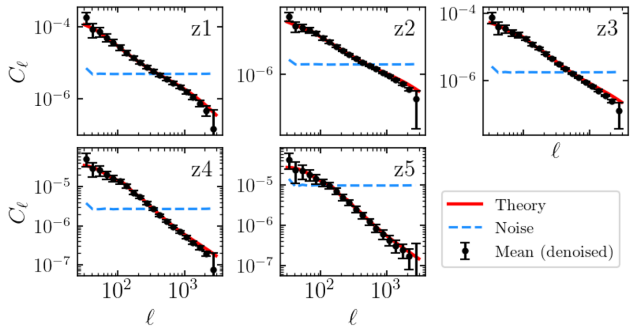

Figure 1. Measured galaxy clustering angular power spectra on the 1200 DES-Y1 FLASK mocks. We show the mean of the noise subtracted measurements along the mock realizations with the 1σ dispersion (black dots), the unbinned theoretical input for the realizations (red line) and the estimated binned noise (dot-dashed blue line) for the five photometric redshift bins.

with the following parameters (which we call FLASK cosmology): $\Omega_m = 0.285$, $\Omega_b = 0.05$, $\sigma_8 = 0.82$, $h = 0.7$, $n_s = 0.96$, and $\sum m_\nu = 0$.

Galaxy maps were generated in five photometric redshift (z_{ph}) bins, with ranges (0.15–0.3), (0.3–0.45), (0.45–0.6), (0.6–0.75), and (0.75–0.9), and with redshift distributions given in Elvin-Poole et al. (2018). The average number density of objects in each tomographic bin are: 0.01337, 0.03434, 0.05094, 0.03297, and 0.00886 arcmin^{-2}. We also adopted a linear bias model with a fixed value for each redshift bin given by $b = 1.45$, 1.55, 1.65, 1.8, and 2.0, respectively.

4.2 Measurements on DES-Y1 mocks

The measurements of the angular power spectrum for the 1200 mocks were performed using `NaMaster`, as described in Section 3. We measured pseudo-C_ℓ's in 20 logarithmic bins with $\ell_{\rm min} = 30$, $\ell_{\rm max} = 3000$ and a resolution of Nside=2048. The DES-Y1 mask was used to compute the coupling matrix to obtain the binned C_ℓ's.

In order to obtain a clean measurement of the clustering signal, we subtracted a noise term assumed to be purely Poissonian. For that, we follow the analytical derivation in Alonso et al. (2019) for the shot noise in the pseudo-C_ℓ measurement, $f_{\rm sky}/\bar{n}_g^i$, where $f_{\rm sky}$ is the covered fraction of the sky, defined by the angular mask, and $\bar{n}_g^i$ the angular density of galaxies in the i-th tomographic redshift bin in units of inverse steradians. Here we use the input average density of galaxies for each redshift bin i for all mocks.

In Fig. 1, we show the average of the 1200 shot-noise subtracted measurements of the auto (same redshift bin) angular power spectrum and compare them with the un-binned input C_ℓ's demonstrating good agreement.

However, one can notice that the first bin in ℓ lies systematically higher than the theoretical input in all five redshift bins. The reason is that the input C_ℓ's are not binned (we show the value of C_ℓ at the centre of the bin). We show in Fig. 2 that properly taking into account binning in the theoretical input C_ℓ's via equation (13) affects only the largest scales and it actually improves the agreement of the first bin. Since these scales will not be considered we will use in the following the theoretical C_ℓ's computed at the centre of the bins in order to increase the computational speed of the likelihood analysis.

The measurements of the real-space correlation function $w(\theta)$ used in this work were performed on the same mocks using the code `TreeCorr` (Jarvis, Bernstein & Jain 2004) with the parameter binslop set to 0.1 and the Landy–Szalay estimator (Landy & Szalay 1993).

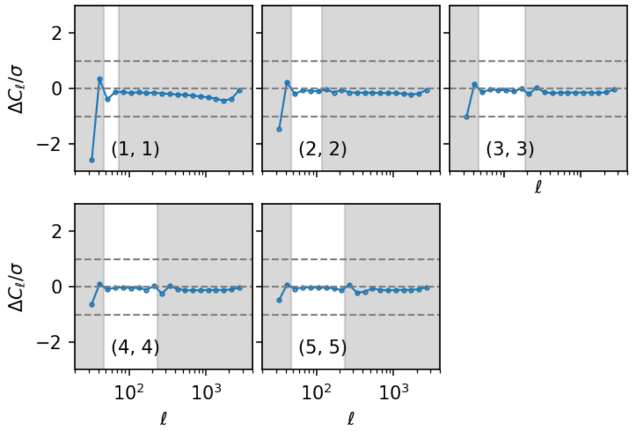

Figure 2. Difference between the interpolated theoretical C_ℓ evaluated at the centre of the bin and the properly binned theoretical prediction measured in terms of its standard deviation for the five redshift bins. The grey regions are the ones excluded by the physical scale cuts (see Section 6).

5 COVARIANCE MATRIX

We use these measurements on the 1200 mocks to estimate a sample covariance matrix for the angular power spectrum, properly taking into account the Hartlap correction factor (Hartlap, Simon & Schneider 2007) for its associated precision matrix. We compare the FLASK covariance matrix with an analytical one generated using CosmoLike with FLASK cosmology which includes non-Gaussian contributions and the mask is treated using the so-called $f_{\rm sky}$ approximation.

We also produced a theoretical covariance matrix using an adapted version of the public code CosmoCov[9] (Fang, Eifler & Krause 2020) based on CosmoLike framework (Krause & Eifler 2017), with configurations consistent with the Y1 3x2pt analyses. This theoretical covariance includes non-Gaussian contributions given by the trispectrum and the supersample covariance. However, it does not contain the effect of the mode coupling induced by the angular mask and also it does not introduce a bandpower binning.

The covariance matrix obtained from lognormal distributions (with its shift parameter fixed by matching perturbation theory predictions for the reduced skewness of the projected density bins at a fiducial smoothing scale of 10 Mpc h^{-1} (see, e.g. Friedrich et al. 2018) has been shown to yield accurate results for DES-Y1 (Krause et al. 2017) and DES-Y3 (Friedrich et al. 2020) two-point observables. Furthermore, it was shown in Friedrich et al. (2020) that the non-connected part of the covariance matrix does not cause significant bias in a cosmological analysis. The main purpose of using these simulations is to have a proper account of the survey geometry in the covariance matrix.

A comparison of the CosmoLike and Flask correlation matrices is shown in Fig. 3 (we have also produced a Gaussian covariance matrix that takes into account the DES-Y1 survey mask using `NaMaster` obtaining similar results). As expected, the FLASK covariance is much noiser than the analytical one. However, we will show in the next section that the impact of these differences in parameter estimation will be negligible after applying scale cuts.

Given the fact that the FLASK covariance is more realistic, taking into account, by construction, the mode coupling from angular

[9] https://github.com/CosmoLike/CosmoCov

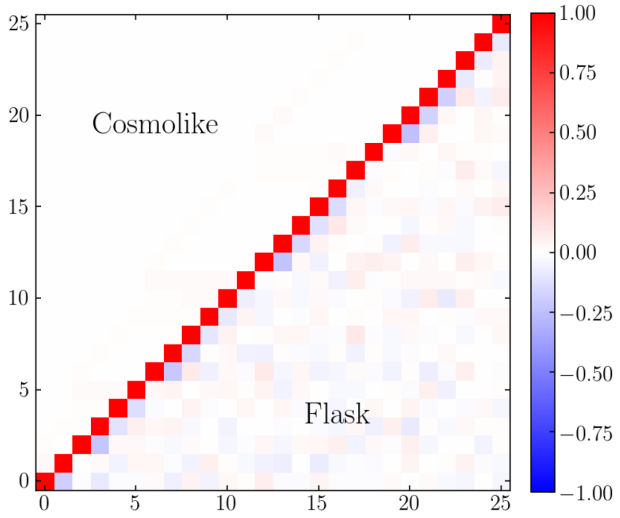

Figure 3. Correlation matrices from the FLASK mocks (lower right triangle) compared to the analytical matrix from CosmoLike using the FLASK cosmology.

masking and proper bandwidth binning, we will be using it as our default choice.

6 ANALYSIS PIPELINE AND SCALE CUTS

6.1 Analysis pipeline

We have developed a pipeline for estimating parameters from the galaxy angular power spectrum based on `CosmoSIS` (Zuntz et al. 2015) using the `MultiNest` sampler (Feroz, Hobson & Bridges 2009; Feroz et al. 2019). We also use the existing DES-Y1 3 × 2-point CosmoSIS pipeline for the angular correlation function in order to compare our results. In order to explore the parameter space, we compute the Likelihood, defined as[10]

$$-2\log\mathcal{L}(\vec{p}) \equiv \chi^2 = \sum_{ij}(D_i - C_{\ell i}(\vec{p}))\ \mathrm{Cov}_{ij}^{-1}(D_j - C_{\ell j}(\vec{p}));\tag{17}$$

where $C_{\ell i}$ is the predicted value at the effective ℓ_i, D_i is the measured data point and Cov is the covariance matrix used in the analysis. Finally, in the scenarios analysed in this work, the best-fitting set of parameters was found using the `MINUIT2` routine (James & Roos 1975).

In this section, we test this pipeline for the average of the FLASK realizations and also for one particular realization. We also study the effect of different scale cuts on the angular power spectrum and use our mocks to determine the scale cuts we will use in the DES-Y1 data.

Our goal is to compare our results to previous DES-Y1 results which focused on the estimate of the galaxy bias parameters b_i, or more precisely on the amplitude of perturbations given by $b_i\sigma_8$. Therefore, we will also concentrate on these quantities.

[10]We assume here a Gaussian likelihood, as justified by the results of Section 7. Although this is not strictly correct for a covariance matrix obtained from mocks (Sellentin & Heavens 2015), it was shown to be a good approximation in realistic cases (Lin et al. 2020). In addition, we have also run chains with a t-distribution likelihood and found negligible differences.

We will run two types of nested sampling chains, depending on the parameters allowed to change: 'quick' chains with only the five bias parameters changing, 'DES-Y1' chains with all 10 nuisance (biases and redshift uncertainties characterized by a shift parameter in the mean of the distribution for each redshift bin). All runs in this section adopt the FLASK cosmology described in Section 4.1.

6.2 Scale cuts

The DES-Y1 analyses defined a scale cut corresponding to a single comoving scale of $R = 8\,h^{-1}$Mpc to ensure that the linear bias model does not bias the estimation of the cosmological parameters in Elvin-Poole et al. (2018). This corresponds to values of $\theta^i_{min} = R/\chi(\langle z^i\rangle)$ given by 43, 27, 20, 16, and 14 arcmin for the five redshift bins with DES-Y1 cosmology. The maximum values are set to $\theta_{max} = 250'$ for all bins.

There is no unique and rigorous way to translate the scale cut in real space to harmonic space and we will test two different relations. We first use a simple relation $\ell = \pi/\theta$ to convert the scale cuts from configuration space to harmonic space and refer to it as '*naive* scale cuts'. This procedure results in the following values for $\ell_{\rm max}$: 251, 400, 540, 675, and 771 for the five redshift bins for DES-Y1 cosmology and $\ell_{\rm min} = 43$ for all bins.

We also use what we call 'physical scale cuts', obtained from a hard cut on the comoving Fourier mode $k_{\rm max} = 1/R$ related to the minimum comoving scale $R = 8\,h^{-1}$ Mpc. This cut is translated to an angular harmonic mode on each tomographic bin using the Limber relation $\ell_{\rm max} = k_{\rm max} \times \chi(\langle z^i\rangle)$, where $\langle z^i\rangle = \int z n(z)\,\mathrm{d}z / \int n(z)\,\mathrm{d}z$ is the mean redshift for the ith tomographic bin of the analysis and $\chi(z)$ the comoving distance computed on the fiducial cosmology of the analysis. Similar approaches were taken in Nicola et al. (2020) and Doux et al. (2020). We fix $k_{\rm max} = 0.125\,h\,\mathrm{Mpc}^{-1}$, which yields $\ell_{\rm max}$ = 80, 127, 172, 215, and 246 for the five redshift bins for DES-Y1 cosmology. We checked these cuts do not change significantly when using a FLASK cosmology. We also keep $\ell_{\rm min} = 43$ for all bins based on the impact of binning for our modelling.

In order to verify whether these scale cuts are effective to mitigate the effects of nonlinear bias we perform a simple χ^2 test comparing two data vectors: a fiducial data vector generated with a linear bias and a data vector contaminated with nonlinear bias. More specifically, we generate a contaminated data vector with an additional quadratic bias parametrized as a function of the linear bias as in Lazeyras et al. (2016). Using the FLASK covariance matrix we find that $\Delta\chi^2 = 0.2$ for the physical cuts, where

$$\Delta\chi^2 = \sum_{qq'}\left(C_q^f - C_q^{b_2}\right)\ \mathrm{Cov}_{qq'}^{-1}\left(C_{q'}^f - C_{q'}^{b_2}\right),\tag{18}$$

well below the criterion $\Delta\chi^2 < 1$ adopted in Abbott et al. (2019a). Hence the nonlinear biases as modelled above are mitigated by the physical scale cuts. Just for comparison, for the naive scale cuts, we find that $\Delta\chi^2 = 14.31$ and therefore this further justifies our fiducial analysis choice for the physical scale cuts.

7 RESULTS ON MOCKS

In order to validate our pipeline, we ran the implemented nested sampling algorithm using as input a random mock realization as well as the average of the set of mocks. We explored the parameter space:

$$\vec{p} = \{b_1,\ b_2,\ b_3,\ b_4,\ b_5,\ \Delta z_1,\ \Delta z_2,\ \Delta z_3,\ \Delta z_4,\ \Delta z_5\ \}\tag{19}$$

where b_i is the constant linear galaxy bias in the redshift shell z_i with a flat prior ($0.8 < b_i < 3.0$), and Δz_i is the respective shift in the

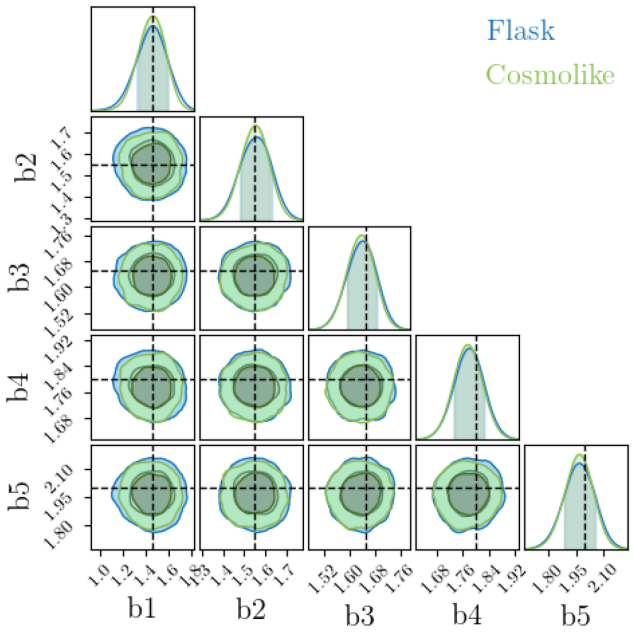

Figure 4. Comparison of the bias constraints to the average of the FLASK mocks using either FLASK (DES-Y1 run) or CosmoLike (quick run) covariance matrices with physical scale cuts for the average of the mocks. Inner (outer) contours are drawn at 68 per cent (95 per cent) of confidence level.

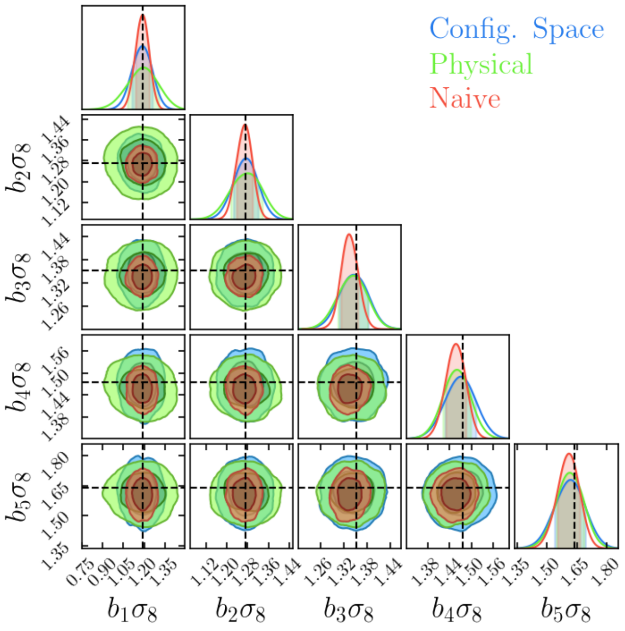

Figure 5. Constraints obtained from the analyses on configuration space and harmonic space for the combination of the five linear bias b_i and σ_8, for the average of the FLASK mocks. The green (red) region are constraints using the physical (naive) scale cut (Section 6.2). Inner (outer) contours are drawn at 68 per cent (95 per cent) of confidence level.

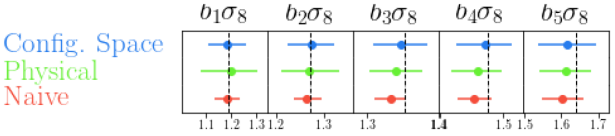

Figure 6. Configuration space and harmonic space constraints (for 2 scale cuts) on $b_i\,\sigma_8$ for the average of the FLASK mocks. The bar represents 68 per cent of confidence level.

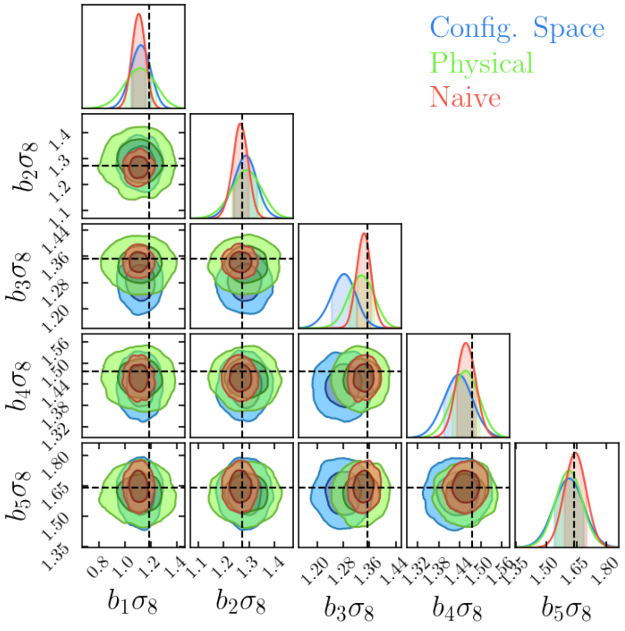

Figure 7. Configuration space and harmonic space contours (for 2 scale cuts) on $b_i\sigma_8$ for a single FLASK mock. Inner (outer) contours are drawn at 68 per cent (95 per cent) of confidence level.

mean of the photometric redshift distribution for each redshift bin i: $n_i(z) \rightarrow n_i(z - \Delta z_i)$. The Gaussian priors are centred in $\Delta z_i = 0$ (for the synthetic data used in this section) and width $\sigma_{\Delta z_i} = \{0.007, 0.007, 0.006, 0.010, 0.010\}$ as in Elvin-Poole et al. (2018).

We use the FLASK covariance matrix as the fiducial one. We show that the CosmoLike theoretical covariance matrix yields very similar results in Fig. 4.[11] In this section, we use the average of the FLASK mocks as a proxy for a noiseless data vector, as used in simulated likelihood analyses (Krause et al. 2017). The use of the FLASK covariance matrix gives the uncertainty one would expect for the real data likelihood analyses, which is the goal of the comparison between the harmonic and configuration space performed in the DES-Y1 data in Section 8. The recovery of unbiased cosmological parameters in this case also shows that the Gaussian likelihood approximation is adequate.

Figs 5 and 6 show the parameter contours for the average of the measurements of the angular correlation function $w(\theta)$ using DES-Y1 cuts and the angular power spectrum C_ℓ on the mocks. In addition to the good agreement between the estimates from configuration and harmonic spaces one can see that the physical scale cuts result in contours more similar to the configuration space (notice that both cuts are consistent with configuration space results at 1σ).

The same general behaviour is seen with the analysis of a single mock, where larger statistical fluctuations are expected, as shown in Figs 7 and 8. The measurements of the combination $b_i\sigma_8$ considering different scale cuts are given in Table 1, for the average of mocks as the data vector, and Table 2, for a single mock realization. In Figs 7 and 8, we show that our pipeline is able to recover the input values from a simulated data vector. Some deviation from the input values are however expected due to statistical fluctuations.

[11]We show only the results for galaxy biases. We have checked that the posterior for the redshift biases are prior-dominated and consistent with zero.

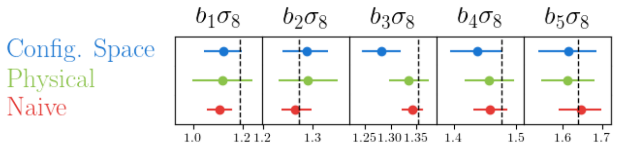

Figure 8. Configuration space and harmonic space constraints (for 2 scale cuts) for a single FLASK mock. The bar represents 68 per cent of confidence level.

As an illustration, for one mock realization, we obtained $\chi^2 = 16.01$ for 16 degrees of freedom at the best-fit parameters, using the Flask covariance matrix and the physical scale cuts. For comparison, the CosmoLike covariance matrix yields $\chi^2 = 20.95$, for the same mock realization and scale cuts, giving $\Delta\chi^2_{C-F} = \chi^2_{\rm CosmoLike} - \chi^2_{\rm Flask} = 4.94$.

This shift can be compared with an analytical approximation for the expectation value and variance of $\Delta\chi^2_{C-F}$, computed following the prescription in Fang et al. (2020),

$$E[\Delta\chi^2_{C-F}] = {\rm Tr}(\mathbf{C}_C^{-1}\mathbf{C}_F) - N_D\ , \tag{20}$$

$${\rm Var}[\Delta\chi^2_{C-F}] = 2N_D + 2{\rm Tr}(\mathbf{C}_C^{-1}\mathbf{C}_F\mathbf{C}_C^{-1}\mathbf{C}_F) - 4{\rm Tr}(\mathbf{C}_C^{-1}\mathbf{C}_F). \tag{21}$$

Here, $\mathbf{C}_{C(F)}$ is the CosmoLike (Flask) covariance and N_D is the number of degrees of freedom, which yields $\Delta\chi^2_{C-F} = 10.67 \pm 4.30$. Hence, the $\Delta\chi^2$ for the particular realization we choose, has a typical deviation from the expected value. Finally, considering the approach in section 7 of Friedrich et al. (2020), we computed the $\Delta\chi^2$ distribution from our set of 1200 mocks, obtaining $\Delta\chi^2 = 9.63 \pm 4.19$ (see Fig. 9). These values corroborate the analytical estimates of χ^2 shift from the different covariance matrices. Detailed investigations of the survey mask effects are discussed in Friedrich et al. (2020).

We notice that the more aggressive physical scale cuts in harmonic space yielded less biased results for the single mock analysis and is more compatible with the real-space analysis. Therefore we opt to choose the physical scale cuts when studying the compatibility between the configuration and harmonic space analyses in the DES-Y1 data in the next section.

8 DES-Y1 RESULTS ON BIAS FROM GALAXY CLUSTERING IN HARMONIC SPACE

We use data taken in the first year (Y1) of DES observations (DES-Y1) (Diehl et al. 2014). In particular, we will follow very closely Elvin-Poole et al. (2018) and use the catalogue, redshift distributions and systematic weights obtained in the configuration space galaxy clustering analysis performed for the DES-Y1 data.

8.1 Data

We use the catalogue created in Elvin-Poole et al. (2018), where details can be found, built from the original so-called 'DES-Y1 Gold' catalogue (Drlica-Wagner et al. 2018), with an area of approximately 1500 deg^2. The galaxy sample in Elvin-Poole et al. (2018) was generated by the redMaGiC algorithm (Rozo et al. 2016), run on DES-Y1 Gold data. The redMaGiC algorithm selects Luminous Red Galaxies (LRGs) in such a way that photometric redshift uncertainties are minimized, and it produces a luminosity-thresholded sample of constant co-moving density. The redMaGiC samples were split into five redshift bins of width $\Delta z = 0.15$ from $z = 0.15$ to $z = 0.9$. After masking and additional cuts, the total number of objects is 653 691 distributed over an area of 1321 deg^2.

8.2 Survey property maps

The number density of galaxies observed is affected by the conditions of the survey, which are described by the survey property maps. DES has produced 21 of these maps for the Y1 season, such as depth, seeing, airmass, etc. The correlation between the galaxy density maps with the survey property maps are a sign of contamination. A so-called weight method was used in Elvin-Poole et al. (2018) in which weights were applied to the galaxy maps in order to decorrelate them from the survey property maps at the $2-\sigma$ level. We use the weights obtained in Elvin-Poole et al. (2018) in our analysis by correcting the pixelized number counts map of galaxies with these weights as multiplicative corrections.

8.3 Angular power spectrum measurements and results in DES-Y1

We follow the analysis described in Sections 4.2 and 6 validated on the lognormal FLASK mocks. For the angular power spectrum results, we use the covariance matrix estimated by the FLASK mocks. We show results from nested sampling DES-Y1 runs using the `MultiNest` sampler (Feroz et al. 2009) for ten parameters (5 galaxy biases and 5 redshift shifts), keeping the other parameters fixed at DES-Y1 cosmology. In Fig. 10 we show that, as with the analysis on the mocks, the use of either Flask or CosmoLike covariances do not significantly bias our results.

Finally, we present our main results in Figs 11 and 12 from a DES-Y1 run applying the physical scale cuts to the angular power spectrum and compare them with results from a similar run in configuration space.

We also present a comparison of the results for galaxy biases for the different redshift bins from our analyses in configuration space and harmonic space with the results from Elvin-Poole et al. (2018) in Fig. 13.

We show in Fig. 14 the DES-Y1 angular power spectrum measurements including the scale cuts compared to the best-fitting predictions.

Fixing the cosmological parameters, we measured the galaxy biases for the harmonic space analysis (with physical scale cut), as shown in Table 3. In order to compare the analyses in harmonic and configuration space, we also used our pipeline to constrain the same set of parameters in configuration space in Fig. 11.

We analyse the goodness-of-fit by computing the reduced χ^2 (equation 17) at best-fitting parameters. For the DES-Y1 data in harmonic space, we obtain $\chi^2 = 28.2$ at the best-fitting set of parameters $\vec{p}$ for $\nu = 26$–10 degrees of freedom. These results yield to a probability to exceed (PTE) of 3.0 per cent. Nevertheless, as remarked in Elvin-Poole et al. (2018), since the five nuisance parameters Δz_i are strongly prior dominated, one can consider here the effective number only the remaining five parameters as the free parameters, which leads in our case to $\nu = 26$–5 and a PTE of 13.5 per cent. The quoted values of PTE shows that the pipeline was able to produce a reasonable fit to the DES-Y1 data in harmonic space. The probability to exceed found by Elvin-Poole et al. (2018) are 1.4 and 4.5 per cent for 10 and 5 free parameters, respectively, and 54 data points. These values are compatible to what we have found in this work.

Table 1. Measurements of galaxy bias for the different redshift bins from the average of mocks, using Flask covariances in three different cases: (i) for the configuration space using the pipeline of this paper, and for harmonic space (ii) *physical* scale cuts and (iii) the *naive* scale cuts (Fig. 5). Harmonic space with physical scale cuts and configuration space have a good agreement between each other.

Model	$b_1\sigma_8$	$b_2\sigma_8$	$b_3\sigma_8$	$b_4\sigma_8$	$b_5\sigma_8$
FLASK cosmology	1.189	1.271	1.353	1.476	1.640
Config. Space	$1.186^{+0.074}_{-0.075}$	$1.274^{+0.047}_{-0.049}$	$1.347^{+0.037}_{-0.039}$	$1.471^{+0.042}_{-0.043}$	$1.617^{+0.077}_{-0.080}$
Physical	$1.194^{+0.100}_{-0.120}$	$1.274^{+0.061}_{-0.059}$	1.340 ± 0.037	$1.458^{+0.038}_{-0.041}$	$1.615^{+0.068}_{-0.071}$
Naive	$1.186^{+0.046}_{-0.050}$	$1.265^{+0.029}_{-0.027}$	1.333 ± 0.022	$1.454^{+0.027}_{-0.026}$	$1.602^{+0.058}_{-0.055}$

Table 2. Measurements of galaxy bias for the different redshift bins from a single mock realization, using Flask covariances in three different cases: (i) for the configuration space using the pipeline of this paper, and for harmonic space (ii) *physical* scale cuts and (iii) the *naive* scale cuts (Fig. 7). Harmonic space with physical scale cuts and configuration space have a good agreement between each other.

Model	$b_1\sigma_8$	$b_2\sigma_8$	$b_3\sigma_8$	$b_4\sigma_8$	$b_5\sigma_8$
FLASK cosmology	1.189	1.271	1.353	1.476	1.640
Config. Space	1.121 ± 0.077	$1.287^{+0.044}_{-0.048}$	$1.282^{+0.038}_{-0.039}$	$1.437^{+0.040}_{-0.044}$	$1.613^{+0.073}_{-0.076}$
Physical	$1.133^{+0.120}_{-0.130}$	$1.287^{+0.061}_{-0.060}$	1.337 ± 0.039	$1.459^{+0.040}_{-0.039}$	$1.619^{+0.075}_{-0.069}$
Naive	$1.104^{+0.054}_{-0.049}$	$1.262^{+0.029}_{-0.028}$	$1.339^{+0.023}_{-0.021}$	$1.451^{+0.028}_{-0.026}$	1.636 ± 0.055

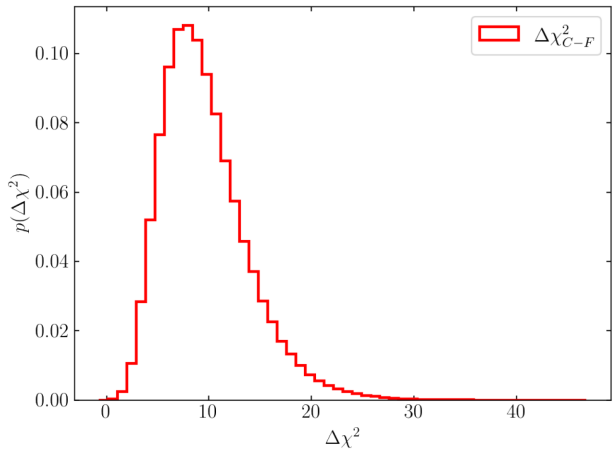

Figure 9. Histogram of $\Delta\chi^2$ for the CosmoLike covariance and the Flask covariance (fiducial) and lognormal datavectors. We computed the χ^2 of mocks by the method described in section 7 of Friedrich et al. (2020). From the resulting distribution of $\Delta\chi^2 = \chi^2_{\rm CosmoLike} - \chi^2_{\rm Flask}$, we obtain $\Delta\chi^2 = 9.63 \pm 4.19$. This value are in agreement to the theoretical estimate (Section 7), namely, $\Delta\chi^2_{C-F} = 10.67 \pm 4.30$.

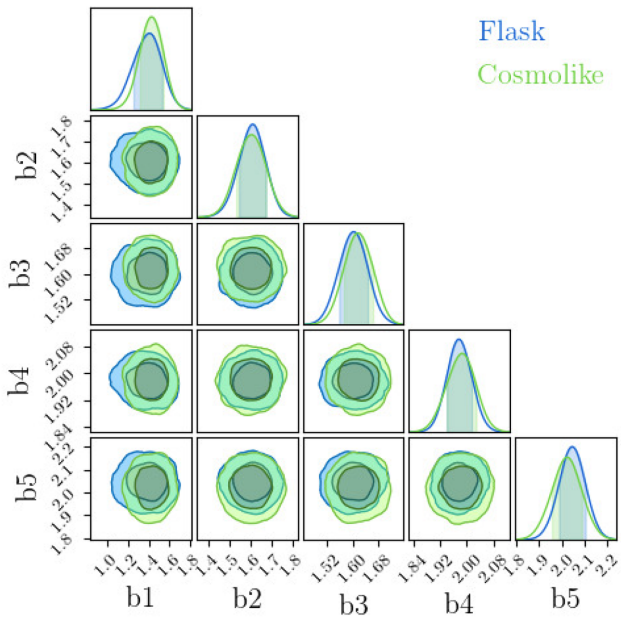

Figure 10. Comparison on the constraints obtained from the analyses on harmonic space using either Flask or CosmoLike covariances.

9 CONCLUSIONS

In this work, we present a pipeline to estimate cosmological parameters from tomographic measurements of the angular power spectrum of galaxy clustering in the DES-Y1 data within the framework of `CosmoSIS` and using several products originally developed by the DES collaboration for the real-space analysis. We focus on the determination of the linear galaxy bias in order to compare with the DES-Y1 analysis of the full-shape angular correlation function in real-space.

We tested the pipeline in a suite of lognormal simulations, devise scale cuts in harmonic space and applied the analysis to DES-Y1 data. We showed that different covariance matrices from FLASK and CosmoLike produce similar constraints. Our analysis makes use of the sharp scale cuts devised for the DES-Y1 real-space analysis adapted to harmonic space. Sharp cuts in configuration space do not map exactly into sharp cuts in harmonic space and we study two possibilities which we call naive and physical scale cuts. We conclude that the latter produce results that are more consistent with the real-space analysis on the mocks. Finally, applying our pipeline to DES-Y1 data We find that our results are consistent with the DES-Y1 real-space analysis of Elvin-Poole et al. (2018).

We are currently working on a complete 3x2pt analyses in harmonic space for the DES-Y1 data and plan to do the same

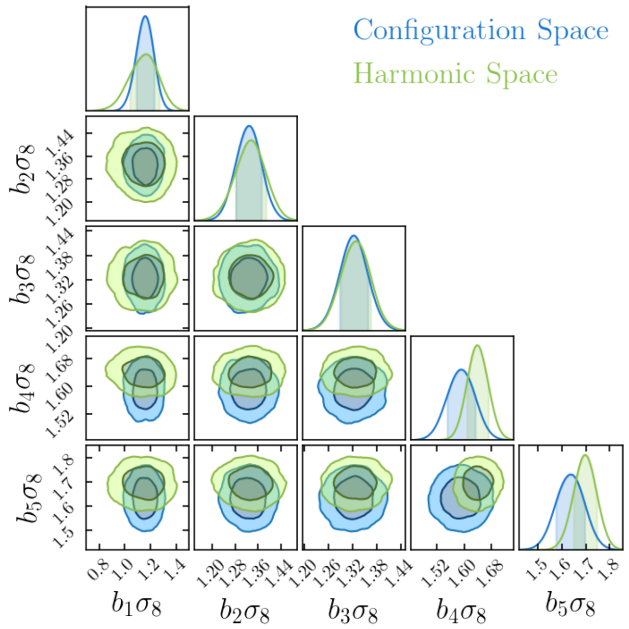

Figure 11. Comparison on the constraints obtained from the analyses on configuration space and harmonic space for the combination of the 5 linear bias b_i and σ_8, for DES-Y1 data. We are using physical cuts for the angular power spectrum. Inner (outer) contours are drawn at 68 per cent (95 per cent) of confidence level.

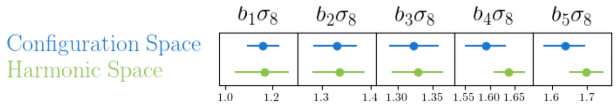

Figure 12. Marginalized results in configuration space and harmonic on $b\sigma_8$ for DES-Y1 data. The error bars represents 68 per cent of confidence level.

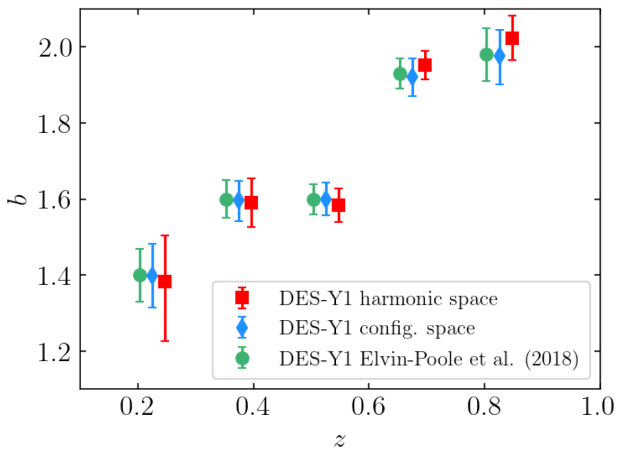

Figure 13. Comparison of the results on galaxy bias for the different redshift bins from our analyses in configuration space and harmonic space and the results from Elvin-Poole et al. (2018) for DES-Y1 data also in configuration space. The error bars represents 68 per cent of confidence level.

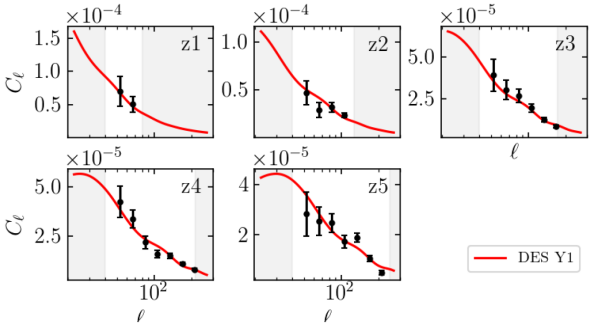

Figure 14. Measurements of angular power spectrum in DES-Y1 compared to a model with the best fit values for galaxy bias. Grey bands are the physical scale cuts.

for DES-Y3 data .[12] These results are an initial step towards a multiprobe analyses using the angular power spectra for the Dark Energy Survey with a goal of demonstrating their compatibility and eventually combining real and harmonic space results.

ACKNOWLEDGEMENTS

We sincerely thank Henrique Xavier for helpful discussions on lognormal mock simulations and the FLASK code.

This research was partially supported by the Laboratório Interinstitucional de e-Astronomia (LIneA), the Brazilian funding agencies CNPq and CAPES, the Instituto Nacional de Ciência e Tecnologia (INCT) e-Universe (CNPq grant 465376/2014-2), and the Sao Paulo State Research Agency (FAPESP) through grants 2019/04881-8 (HC) and 2017/05549-1 (AT). The authors acknowledge the use of computational resources from LIneA, the Center for Scientific Computing (NCC/GridUNESP) of the Sao Paulo State University (UNESP), and from the National Laboratory for Scientific Computing (LNCC/MCTI, Brazil), where the SDumont supercomputer (`sdumont.lncc.br`) was used. This research used resources of the National Energy Research Scientific Computing Center (NERSC), a U.S. Department of Energy Office of Science User Facility operated under Contract No. DE-AC02-05CH11231.

This paper has gone through internal review by the DES collaboration. Funding for the DES Projects has been provided by the U.S. Department of Energy, the U.S. National Science Foundation, the Ministry of Science and Education of Spain, the Science and Technology Facilities Council of the United Kingdom, the Higher Education Funding Council for England, the National Center for Supercomputing Applications at the University of Illinois at Urbana-Champaign, the Kavli Institute of Cosmological Physics at the University of Chicago, the Center for Cosmology and Astro-Particle Physics at the Ohio State University, the Mitchell Institute for Fundamental Physics and Astronomy at Texas A&M University, Financiadora de Estudos e Projetos, Fundação Carlos Chagas Filho de Amparo à Pesquisa do Estado do Rio de Janeiro, Conselho Nacional de Desenvolvimento Científico e Tecnológico and the Ministério da Ciência, Tecnologia e Inovação, the Deutsche Forschungsgemeinschaft, and the Collaborating Institutions in the Dark Energy Survey.

[12] After the completion of this work, a preprint appeared with an analysis of DES-Y1 public data in harmonic space with a model for galaxy bias based on Effective Field Theory (Hadzhiyska et al. 2021) more sophisticated than the fiducial one used in DES-Y1.

Table 3. Measurements of galaxy bias for the different redshift bins from DES-Y1 data: (i) for the configuration space using the pipeline of this paper and (ii) for harmonic space with *physical* scale cuts (Fig. 11). Harmonic space with physical scale cuts and configuration space have compatible measurements.

Model	$b_1\sigma_8$	$b_2\sigma_8$	$b_3\sigma_8$	$b_4\sigma_8$	$b_5\sigma_8$
Config. Space	$1.160^{+0.070}_{-0.069}$	$1.325^{+0.042}_{-0.047}$	1.327 ± 0.035	$1.593^{+0.041}_{-0.042}$	$1.639^{+0.057}_{-0.063}$
Harmonic Space	$1.147^{+0.100}_{-0.130}$	$1.319^{+0.053}_{-0.054}$	$1.314^{+0.036}_{-0.038}$	$1.618^{+0.032}_{-0.030}$	$1.677^{+0.049}_{-0.048}$

The Collaborating Institutions are Argonne National Laboratory, the University of California at Santa Cruz, the University of Cambridge, Centro de Investigaciones Energéticas, Medioambientales y Tecnológicas-Madrid, the University of Chicago, University College London, the DES-Brazil Consortium, the University of Edinburgh, the Eidgenössische Technische Hochschule (ETH) Zürich, Fermi National Accelerator Laboratory, the University of Illinois at Urbana-Champaign, the Institut de Ciències de l'Espai (IEEC/CSIC), the Institut de Física d'Altes Energies, Lawrence Berkeley National Laboratory, the Ludwig-Maximilians Universität München and the associated Excellence Cluster Universe, the University of Michigan, the National Optical Astronomy Observatory, the University of Nottingham, The Ohio State University, the University of Pennsylvania, the University of Portsmouth, SLAC National Accelerator Laboratory, Stanford University, the University of Sussex, Texas A&M University, and the OzDES Membership Consortium.

Based in part on observations at Cerro Tololo Inter-American Observatory at NSF's NOIRLab (NOIRLab Prop. ID 2012B-0001; PI: J. Frieman), which is managed by the Association of Universities for Research in Astronomy (AURA) under a cooperative agreement with the National Science Foundation.

The DES data management system is supported by the National Science Foundation under grant numbers AST-1138766 and AST-1536171. The DES participants from Spanish institutions are partially supported by MINECO under grants AYA2015-71825, ESP2015-66861, FPA2015-68048, SEV-2016-0588, SEV-2016-0597, and MDM-2015-0509, some of which include ERDF funds from the European Union. IFAE is partially funded by the CERCA program of the Generalitat de Catalunya. Research leading to these results has received funding from the European Research Council under the European Union's Seventh Framework Program (FP7/2007-2013) including ERC grant agreements 240672, 291329, and 306478.

This manuscript has been authored by Fermi Research Alliance, LLC under Contract No. DE-AC02-07CH11359 with the U.S. Department of Energy, Office of Science, Office of High Energy Physics.

This work made use of the software packages `ChainConsumer` (Hinton 2016), `matplotlib` (Hunter 2007), and `numpy` (Harris et al. 2020).

DATA AVAILABILITY

The DES Y1 catalogue is available in the Dark Energy Survey Data Management (DESDM) system at the National Center for Supercomputing Applications (NCSA) at the University of Illinois. It can be accessed at https://des.ncsa.illinois.edu/releases/y1a1/key-catalogs/key-redmagic. The pipeline used for the measurement is publicly available at https://github.com/hocamachoc/3x2hs_measurements. Synthetic data produced by the analysis presented here can be shared on request to the corresponding author.

REFERENCES

Abbott T. M. C. et al., 2018, Phys. Rev. D, 98, 043526
Abbott T. M. C. et al., 2019a, Phys. Rev. D, 99, 123505
Abbott T. et al., 2019b, MNRAS, 483, 4866
Alonso D., Sanchez J., Slosar A., LSST Dark Energy Science Collaboration, 2019, MNRAS, 484, 4127
Balaguera-Antolínez A., Bilicki M., Branchini E., Postiglione A., 2018, MNRAS, 476, 1050
Bautista J. E. et al., 2021, MNRAS, 500, 736
Bilicki M., Jarrett T. H., Peacock J. A., Cluver M. E., Steward L., 2014, ApJS, 210, 9
Camacho H. et al., 2019, MNRAS, 487, 3870
de Mattia A. et al., 2020, MNRAS, 501, 5616
Diehl H. et al., 2014, Proc. SPIE Int. Soc. Opt. Eng., 9149, 91490V
Doux C. et al., 2020, 503, 3796
Drlica-Wagner A. et al., 2018, ApJS, 235, 33
eBOSS Collaboration, 2020, Phys. Rev. D., 103, 083533
Elvin-Poole J. et al., 2018, Phys. Rev. D, 98, 042006
Fang X., Eifler T., Krause E., 2020, MNRAS, 497, 2699
Feroz F., Hobson M., Bridges M., 2009, MNRAS, 398, 1601
Feroz F., Hobson M., Cameron E., Pettitt A., 2019, Open J. Astrophys., 2, 10
Friedrich O. et al., 2018, Phys. Rev. D, 98, 023508
Friedrich O. et al., 2020, preprint (arXiv:2012.08568)
Frieman J., Turner M., Huterer D., 2008, ARA&A, 46, 385
Gil-Marín H. et al., 2020, MNRAS, 498, 2492
Hadzhiyska B., García-García C., Alonso D., Nicola A., Slosar A., 2021, preprint (arXiv:2103.09820)
Hamana T. et al., 2020, PASJ, 72, 16
Harris C. R. et al., 2020, Nature, 585, 357
Hartlap J., Simon P., Schneider P., 2007, A&A, 464, 399
Heymans C. et al., 2021, A&A, 646, A140
Hikage C. et al., 2019, PASJ, 71, 43
Hinton S. R., 2016, J. Open Source Softw., 1, 00045
Hivon E., Gorski K. M., Netterfield C. B., Crill B. P., Prunet S., Hansen F., 2002, ApJ, 567, 2
Hou J. et al., 2021, MNRAS, 500, 1201
Hunter J. D., 2007, Comput. Sci. Eng., 9, 90
James F., Roos M., 1975, Comput. Phys. Commun., 10, 343
Jarvis M., Bernstein G., Jain B., 2004, MNRAS, 352, 338
Köhlinger F. et al., 2017, MNRAS, 471, 4412
Krause E., Eifler T., 2017, MNRAS, 470, 2100
Krause E. et al., 2017, preprint (arXiv:1706.09359)
Landy S. D., Szalay A. S., 1993, ApJ, 412, 64
Lazeyras T., Wagner C., Baldauf T., Schmidt F., 2016, J. Cosmol. Astropart. Phys., 02, 018
Limber D. N., 1953, ApJ, 117, 134
Lin C.-H., Harnois-Déraps J., Eifler T., Pospisil T., Mandelbaum R., Lee A. B., Singh S., LSST Dark Energy Science Collaboration, 2020, MNRAS, 499, 2977
Loureiro A. et al., 2019, MNRAS, 485, 326
LoVerde M., Afshordi N., 2008, Phys. Rev. D, 78, 123506
Neveux R. et al., 2020, MNRAS, 499, 210
Nicola A. et al., 2020, J. Cosmol. Astropart. Phys., 2020, 044
Prat J. et al., 2018, Phys. Rev. D, 98, 042005
Rozo E. et al., 2016, MNRAS, 461, 1431
Salazar-Albornoz S. et al., 2017, MNRAS, 468, 2938

Sellentin E., Heavens A. F., 2015, MNRAS, 456, L132
Smith R. E. et al., 2003, MNRAS, 341, 1311
Takahashi R., Sato M., Nishimichi T., Taruya A., Oguri M., 2012, ApJ, 761, 152
Tamone A. et al., 2020, MNRAS, 499, 5527
Troxel M. et al., 2018, Phys. Rev. D, 98, 043528
van Uitert E. et al., 2018, MNRAS, 476, 4662
Verde L., Treu T., Riess A. G., 2019, Nat. Astron., 3, 891
Xavier H. S., Abdalla F. B., Joachimi B., 2016, MNRAS, 459, 3693
Zuntz J. et al., 2015, Astron. Comput., 12, 45

[1]*Instituto de Física Teórica, Universidade Estadual Paulista, São Paulo 01140-070, Brazil*
[2]*Laboratório Interinstitucional de e-Astronomia - LIneA, Rua Gal. José Cristino 77, Rio de Janeiro, RJ 20921-400, Brazil*
[3]*Departamento de Física Matemática, Instituto de Física, Universidade de São Paulo, CP 66318, São Paulo, SP 05314-970, Brazil*
[4]*ICTP South American Institute for Fundamental Research Instituto de Física Teórica, Universidade Estadual Paulista, São Paulo 01140-070, Brazil*
[5]*Department of Physics, University of Michigan, Ann Arbor, MI 48109, USA*
[6]*Department of Physics and Astronomy, University of Pennsylvania, Philadelphia, PA 19104, USA*
[7]*Center for Cosmology and Astro-Particle Physics, The Ohio State University, Columbus, OH 43210, USA*
[8]*Department of Physics, The Ohio State University, Columbus, OH 43210, USA*
[9]*Department of Astronomy/Steward Observatory, University of Arizona, 933 North Cherry Avenue, Tucson, AZ 85721-0065, USA*
[10]*Kavli Institute for Cosmology, University of Cambridge, Madingley Road, Cambridge CB3 0HA, UK*
[11]*Churchill College, University of Cambridge, Cambridge CB3 0DS, UK*
[12]*Department of Physics, Stanford University, 382 Via Pueblo Mall, Stanford, CA 94305, USA*
[13]*Kavli Institute for Particle Astrophysics & Cosmology, P.O. Box 2450, Stanford University, Stanford, CA 94305, USA*
[14]*Institut d'Estudis Espacials de Catalunya (IEEC), E-08034 Barcelona, Spain*
[15]*Institute of Space Sciences (ICE, CSIC), Campus UAB, Carrer de Can Magrans, s/n, E-08193 Barcelona, Spain*
[16]*Fermi National Accelerator Laboratory, P.O. Box 500, Batavia, IL 60510, USA*
[17]*Instituto de Fisica Teorica UAM/CSIC, Universidad Autonoma de Madrid, E-28049 Madrid, Spain*
[18]*CNRS, UMR 7095, Institut d'Astrophysique de Paris, F-75014 Paris, France*
[19]*Sorbonne Universités, UPMC Univ Paris 06, UMR 7095, Institut d'Astrophysique de Paris, F-75014 Paris, France*
[20]*Department of Physics & Astronomy, University College London, Gower Street, London WC1E 6BT, UK*
[21]*SLAC National Accelerator Laboratory, Menlo Park, CA 94025, USA*
[22]*Center for Astrophysical Surveys, National Center for Supercomputing Applications, 1205 West Clark St., Urbana, IL 61801, USA*
[23]*Department of Astronomy, University of Illinois at Urbana-Champaign, 1002 W. Green Street, Urbana, IL 61801, USA*
[24]*Institut de Física d'Altes Energies (IFAE), The Barcelona Institute of Science and Technology, Campus UAB, E-08193 Bellaterra (Barcelona), Spain*
[25]*Physics Department, 2320 Chamberlin Hall, University of Wisconsin-Madison, 1150 University Avenue Madison, WI 53706-1390, USA*
[26]*Department of Astronomy and Astrophysics, University of Chicago, Chicago, IL 60637, USA*
[27]*Kavli Institute for Cosmological Physics, University of Chicago, Chicago, IL 60637, USA*
[28]*Astronomy Unit, Department of Physics, University of Trieste, via Tiepolo 11, I-34131 Trieste, Italy*
[29]*INAF-Osservatorio Astronomico di Trieste, via G. B. Tiepolo 11, I-34143 Trieste, Italy*
[30]*Institute for Fundamental Physics of the Universe, via Beirut 2, I-34014 Trieste, Italy*
[31]*Observatório Nacional, Rua Gal. José Cristino 77, Rio de Janeiro, RJ 20921-400, Brazil*
[32]*Department of Physics, IIT Hyderabad, Kandi, Telangana 502285, India*
[33]*Santa Cruz Institute for Particle Physics, Santa Cruz, CA 95064, USA*
[34]*Department of Astronomy, University of Michigan, Ann Arbor, MI 48109, USA*
[35]*Institute of Theoretical Astrophysics, University of Oslo, P.O. Box 1029 Blindern, NO-0315 Oslo, Norway*
[36]*School of Mathematics and Physics, University of Queensland, Brisbane, QLD 4072, Australia*
[37]*Center for Astrophysics | Harvard & Smithsonian, 60 Garden Street, Cambridge, MA 02138, USA*
[38]*Department of Applied Mathematics and Theoretical Physics, University of Cambridge, Cambridge CB3 0WA, UK*
[39]*Department of Astrophysical Sciences, Princeton University, Peyton Hall, Princeton, NJ 08544, USA*
[40]*Institució Catalana de Recerca i Estudis Avançats, E-08010 Barcelona, Spain*
[41]*Institute of Astronomy, University of Cambridge, Madingley Road, Cambridge CB3 0HA, UK*
[42]*Centro de Investigaciones Energéticas, Medioambientales y Tecnológicas (CIEMAT), Madrid 28040, Spain*
[43]*School of Physics and Astronomy, University of Southampton, Southampton SO17 1BJ, UK*
[44]*Computer Science and Mathematics Division, Oak Ridge National Laboratory, Oak Ridge, TN 37831, USA*

This paper has been typeset from a TEX/LATEX file prepared by the author.